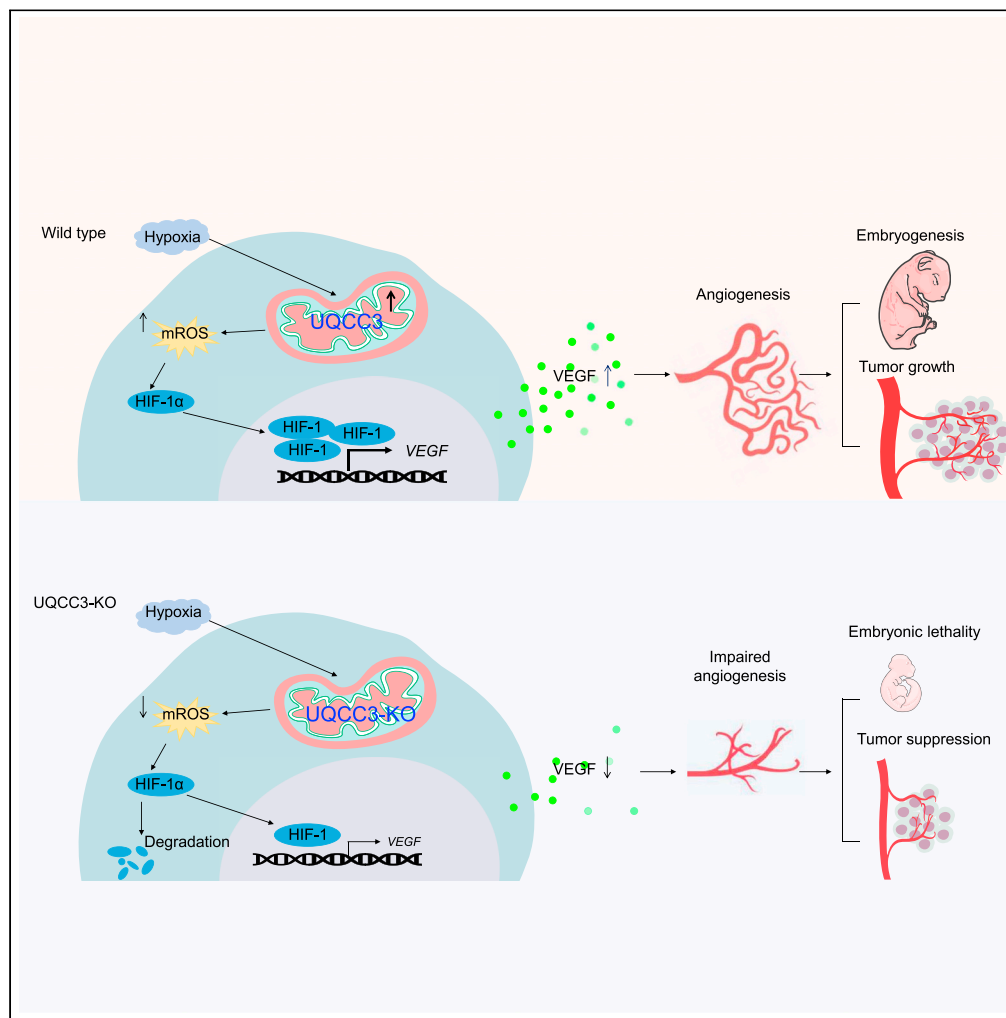


Article

Mitochondrial UQC3 controls embryonic and tumor angiogenesis by regulating VEGF expression



Guimin Zhang,
Binrui Liu, Yun
Yang, ..., Rong Li,
Hongxin Deng,
Hanshuo Yang

yangyun@scu.edu.cn (Y.Y.)
yhansh@scu.edu.cn (H.Y.)

Highlights

Uqc3 homozygous mutant inhibits angiogenesis and causes embryonic lethality in mice

UQC3 deletion inhibits tumor angiogenesis and delays tumor growth

UQC3 regulates angiogenesis through the ROS/HIF/VEGF pathway

UQC3 expression is correlated with the progression and prognosis of tumor patients

Zhang et al., *iScience* 26,
107370
August 18, 2023 © 2023 The
Author(s).
[https://doi.org/10.1016/
j.isci.2023.107370](https://doi.org/10.1016/j.isci.2023.107370)



Article

Mitochondrial UQCC3 controls embryonic and tumor angiogenesis by regulating VEGF expression

Guimin Zhang,^{1,4} Binrui Liu,^{1,4} Yun Yang,^{1,4,*} Shuo Xie,¹ Lingcheng Chen,¹ Hui Luo,¹ Jian Zhong,¹ Yinhao Wei,¹ Fengzhu Guo,² Jia Gan,³ Fan Zhu,¹ Lin Xu,¹ Qiqi Li,¹ Yuge Shen,¹ Huajin Zhang,¹ Yan Liu,¹ Rong Li,¹ Hongxin Deng,¹ and Hanshuo Yang^{1,5,*}

SUMMARY

Mitochondria play important roles in angiogenesis. However, the mechanisms remain elusive. In this study, we found that mitochondrial ubiquinol-cytochrome c reductase complex assembly factor 3 (UQCC3) is a key regulator of angiogenesis. TALEN-mediated knockout of *Uqcc3* in mice caused embryonic lethality at 9.5–10.5 days postcoitum, and vessel density was dramatically reduced. Similarly, knockout of *uqcc3* in zebrafish induced lethality post-fertilization and impaired vascular development. Knockout of UQCC3 resulted in slower tumor growth and angiogenesis. Mechanistically, UQCC3 was upregulated under hypoxia, promoted reactive oxygen species (ROS) generation, enhanced HIF-1 α stability and increased VEGF expression. Finally, higher expression of UQCC3 was associated with poor prognosis in multiple types tumors, implying a role for UQCC3 in tumor progression. In conclusion, our findings highlight the important contribution of UQCC3 to angiogenesis under both physiological and pathological conditions, indicating the potential of UQCC3 as a therapeutic target for cancer.

INTRODUCTION

Angiogenesis is crucial for embryonic development and tumor progression, and a better understanding of the angiogenic process may facilitate the development of more effective cancer therapies.^{1–3} VEGF is a master regulator of angiogenesis in both developmental and pathological contexts.⁴ HIF-1 α , an oxygen concentration-sensitive molecule, induces the expression of a number of angiogenic genes, including VEGF. Under normoxic conditions, HIF-1 α is hydroxylated by prolyl-4-hydroxylase domain (PHD) proteins and subsequently degraded by the ubiquitin-proteasome pathway. Under hypoxic conditions, HIF-1 α is not degraded but translocates into the nucleus and binds HIF-1 β , activating the transcription of downstream pro-angiogenic factors.^{5,6} HIF-1 α stability is influenced by multiple signals, including hypoxia-induced reactive oxygen species (ROS) as a key regulator.⁷ The downstream mechanisms of VEGF-induced angiogenesis have been extensively studied,^{8,9} however the upstream regulatory mechanisms governing HIF-1 α – VEGF expression are less well understood.

Mitochondria sense fluctuations in oxygen availability in tissue, coordinating changes in energy metabolism and ROS generation to maintain an internal environment capable of sustaining an organism. The stability and activity of HIF-1 α and mitochondria are closely interrelated.¹⁰ For example, the mitochondrial electron transport chain (ETC) complexes are believed to regulate the stability of HIF-1 α mainly via oxygen consumption and ROS generation.¹¹ During mitochondrial respiration, electrons are transferred via ETCs and then shuttled onto the final electron acceptor, oxygen. Oxygen is reduced to water at complex IV, but 2%–3% of the consumed oxygen is incompletely reduced, leading to the production of ROS, which then stabilize the HIF-1 α protein.¹² Blocking the respiratory chain reduces oxygen consumption and increases the oxygen concentration in the cellular microenvironment, leading to the degradation of HIF-1 α , mediated by PHD proteins.¹⁰ Cells lacking mitochondrial DNA and electron transport activity fail to increase ROS or upregulate HIF-1 α target genes during hypoxia.¹³ For example, respiratory complex I deficiency caused by knockout of nuclear-encoded NDUFS3 leads to PHD-mediated degradation of HIF-1 α .^{14,15}

¹Department of Biotherapy, Cancer Center and State Key Laboratory of Biotherapy, West China Hospital, Sichuan University, Chengdu 610041, China

²Department of Medical Oncology, Beijing Hospital, National Center of Gerontology, Institute of Geriatric Medicine, Chinese Academy of Medical Sciences, Beijing 100730, China

³Department of Pathology, Xinqiao Hospital, Third Military Medical University, Chongqing 400037, P.R.China

⁴These authors contributed equally

⁵Lead contact

*Correspondence:

yangyun@scu.edu.cn (Y.Y.),

yhansh@scu.edu.cn (H.Y.)

<https://doi.org/10.1016/j.isci.2023.107370>



Moreover, loss of complex II activities caused by succinate dehydrogenase mutation results in succinate accumulation, which has been shown to inhibit the activity of PHD proteins and subsequently induce HIF-1 α stabilization.^{16,17} Mitochondrial complex III has been identified as the main producer of ROS within the mitochondrial respiratory chain.¹⁸ The release of mitochondrial ROS in hypoxic conditions stabilizes HIF-1 α via a mechanism dependent on complex III.¹⁹ Inhibiting complex III can block the generation of mitochondrial ROS and inhibit the stability and transcriptional activity of HIF-1 α in hypoxia; these effects lead to the suppression of angiogenesis, which coincides with decreased VEGF levels.^{20,21} These findings suggest that mitochondrial ETC complexes are critical for HIF-1 α stability and angiogenesis.

Ubiquinol-cytochrome c reductase complex assembly factor 3 (UQCC3, also known as C11orf83), is involved in the early assembly and stability of mitochondrial respiratory chain supercomplexes, including the III/IV and I/III/IV supercomplexes.^{22,23} UQCC3 interacts strongly with the core subunits of complex III and forms part of the co-ordinator of mitochondrial cytochrome b (CYTB) complex during mammalian complex III assembly.²⁴ Deletion of UQCC3 results in significantly reduced levels of complex III and its supercomplexes. Patients bearing UQCC3 homozygous mutations exhibit typical mitochondrial defect disease-related symptoms, such as lactic acidosis, hypoglycemia, hypotonia, developmental delay, and severe psychomotor developmental impairment.²³ In our previous studies, we revealed that UQCC3 was critical for the generation of ROS in mitochondria. In hypoxic tumor cells, UQCC3 formed a positive feedback loop with ROS to maintain mitochondrial homeostasis and stabilize HIF-1 α , thereby reprogramming metabolism under hypoxic conditions.²⁵ These findings prompted us to speculate whether UQCC3 play an important role in angiogenesis by regulating VEGF expression during embryonic development and tumor growth.

Here, we investigated the function of UQCC3 in angiogenesis in multiple *Uqcc3*-deficient animal models, including a TALEN-mediated knockout mouse, CRISPR/Cas9-mediated knockout zebrafish, and a liver-specific conditional (Cre-loxp system) *Uqcc3*-knockout mouse model. These models showed the indispensable role of *Uqcc3* in angiogenesis. Moreover, knockout of UQCC3 in tumor cells significantly inhibited tumor growth and impaired tumor angiogenesis *in vivo*. Mechanistically, our findings indicated that the upregulation of UQCC3 in hypoxia promoted angiogenesis by enhancing ROS generation, stabilizing HIF-1 α , and inducing VEGF expression. In addition, UQCC3 expression was higher in tumor tissues than in the corresponding normal tissues and were associated with poor prognosis in multiple types of human tumors. Taken together, our data reveal hitherto unknown roles of UQCC3 in critical steps of angiogenesis during embryonic development and tumor growth and indicate the potential of UQCC3 as a therapeutic target for cancer.

RESULTS

Uqcc3 homozygous mutant causes embryonic lethality in mice

To investigate the *in vivo* roles of *Uqcc3* under normal conditions, we generated mutant mice deficient in *Uqcc3* (Figure 1A). The genotype of mutant mice was analyzed via agarose gel electrophoresis and direct sequencing (Figures S1A and S1B). The amino acid sequence of UQCC3 was also altered (Figure S1C). Mice heterozygous for the targeted allele of *Uqcc3* (*Uqcc3*^{+/-}) were viable and fertile with no obvious abnormalities (Figures S1D and S1E). These mice were intercrossed to generate homozygous mice deficient in *Uqcc3* (Figure S1F). From each line of heterozygous mice that were intercrossed, the ratio of the three genotypes was not within the expected mendelian range. We did not detect any homozygous pups at weaning (Figure 1B), suggesting that *Uqcc3* homozygous deletion causes embryonic lethality. To further assess this hypothesis, we studied the fertilization ability of mouse oocytes by culturing them and performing *in vitro* fertilization (IVF). However, we found that *Uqcc3* deletion does not cause embryo death from fertilization to blastocyst (Figure 1C). We then analyzed and genotyped embryos at different stages of *in vivo* development, from 6.5 to 15.5 days postcoitum (dpc). We found that at 8.5 dpc, the number of embryos of different genotypes followed the expected mendelian ratios, suggesting that *Uqcc3* knockout does not affect implantation and decidualization. However, at 9.5 and 10.5 dpc, the number of viable embryos carrying the homozygous mutation was decreased, and at 11.5 dpc, none of them carried the mutation in homozygosis (Figure 1C). Moreover, analysis of nonviable mutant embryos at 9.5 dpc showed a clear reduction in size when compared with their littermate controls (Figure 1D), suggesting that their development was arrested. To clarify the embryonic lethality of *Uqcc3*^{-/-}, we performed comparative histological analysis of embryos from the three genotypes. *Uqcc3*^{-/-} embryos showed a marked decrease in growth, being much smaller than their littermate controls and exhibiting incomplete formation of organs (Figure 1E), indicating that *Uqcc3* deletion causes damage to organ formation during embryo development.

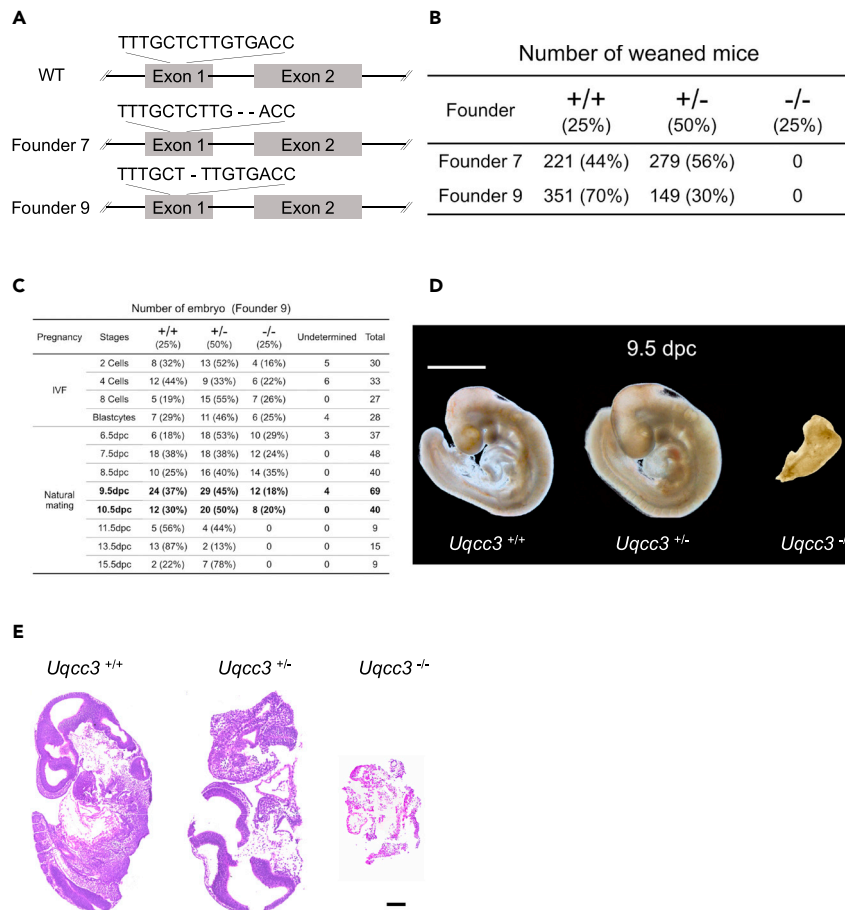


Figure 1. Mutant *Uqcc3* caused a mid-gestation embryonic lethal phenotype in homozygous mutant mice

(A) Illustration of a CRISPR/Cas9-based targeting strategy to delete a 2/1-bp sequence in *Uqcc3* exon 1.

(B) After genetic identification, the results of the crossing were reported in a table (progeny).

(C) After *in vitro* fertilization (IVF), cells were cultured from 2 cells to blastocyst, and natural mating was performed from E6.5 to E15.5. The genotype results are reported in a table.

(D) Light microscope images of E9.5 *Uqcc3*^{+/+}, *Uqcc3*^{+/-}, and *Uqcc3*^{-/-} embryos illustrate the growth delay of the *Uqcc3* KO embryos. Scale bar: 1 mm.

(E) Hematoxylin/eosin staining was performed on the sagittal sections of E9.5 *Uqcc3*^{+/+}, *Uqcc3*^{+/-}, and *Uqcc3*^{-/-} embryos, highlighting the morphology and abnormal development of the *Uqcc3* KO embryos. Scale bar: 200 μm.

***Uqcc3* deletion impair embryonic angiogenesis**

Development of the vascular system is essential for embryonic development [13]. Angiogenesis occurs early in development; in fact, the vascular system is the first functional organ that develops in an embryo.^{26,27} We next analyzed E9.5 yolk sacs of *Uqcc3*^{-/-} embryos. The wild-type yolk sacs at E9.5 contained many large, branched blood vessels with a well-organized structure (Figure 2A, left). In contrast, the yolk sacs of *Uqcc3*-deficient embryos were devoid of such blood vessels (Figure 2A, right). Moreover, the mutant embryos were significantly smaller than their wild-type littermates, and no obvious blood vessels were observed in the embryos (Figure 2B). To confirm the lack of blood vessels, we performed whole-mount immunofluorescence staining of E9.5 embryos with anti-CD31, an antibody specific for platelet endothelial cell adhesion molecule. Wild-type embryos contained large, well-branched blood vessels, whereas mutant embryos contained only honeycomb-like primordial blood plexus. Furthermore, *Uqcc3* deletion significantly reduced vessel branch points (Figure 2C). In addition, we detected cell apoptosis with TUNEL staining and found a significant increase in apoptotic cells in *Uqcc3*-deficient embryos (Figure 2D). Next, we investigated angiogenesis by taking advantage of the superiority of live optically transparent transgenic zebrafish larvae of Tg (flk1: EGFP). We injected zebrafish embryos with sgRNA to knockout *uqcc3* and found that angiogenesis was impaired in *uqcc3*-knockout zebrafish (Figure 2E). We

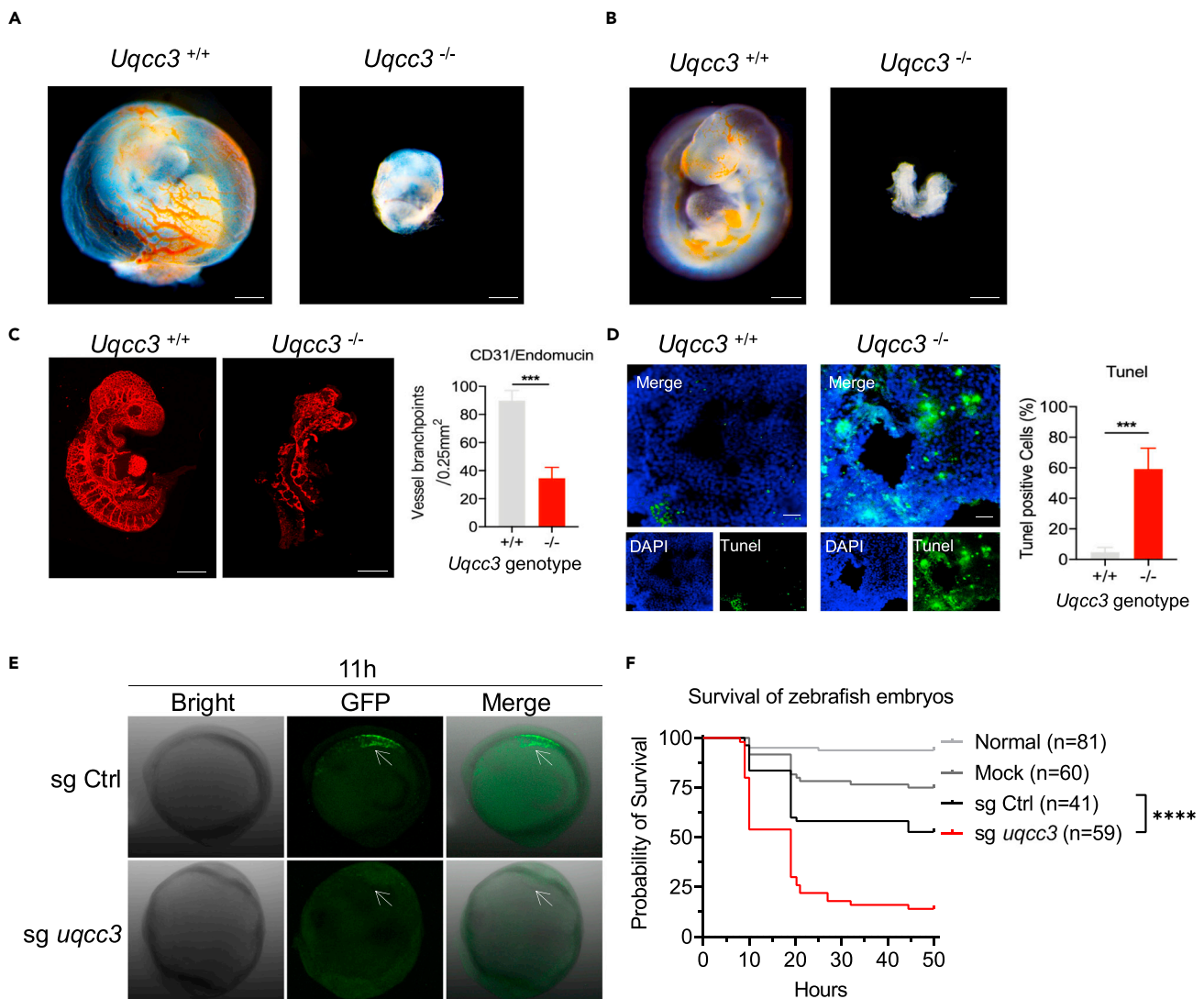


Figure 2. *Uqcc3* deficiency impaired angiogenesis in mice and zebrafish embryos development

(A) Gross examination of yolk sac at E9.5 during the development of *Uqcc3*^{+/+} and *Uqcc3*^{-/-} embryos. (Scale bars, 500 μ m).

(B) Gross examination of whole embryos at E9.5 during the development of *Uqcc3*^{+/+} and *Uqcc3*^{-/-} embryos. (Scale bars, 500 μ m).

(C) Whole-mount staining of E9.5 embryos using antibodies against the endothelial marker CD31 revealed defects in the vascular system of the *Uqcc3*^{-/-} embryo. The control embryo has a normally organized and branched network of vessels. Scale bar = 500 μ m. Data are represented as means \pm SEM.

***p < 0.001, Student's t test.

(D) Embryonic cell apoptosis was detected using TUNEL staining and analyzed by confocal microscopy in *Uqcc3*^{+/+} and *Uqcc3*^{-/-} embryos, and TUNEL-positive cells were analyzed using ImageJ (n = 3 in each group). Scale bar: 200 μ m. Data are represented as means \pm SEM. ***p < 0.001, Student's t test.

(E) Representative images of blood vessels in Tg (flk1: EGFP) zebrafish embryos during early stages (11h) of development in *uqcc3*^{+/+} and *uqcc3*^{-/-} embryos. Scale bar = 50 μ m.

(F) Effect of *uqcc3* knockout on the survival rate of zebrafish embryos over 50 hpf. ****p < 0.0001, Kaplan-Meier.

also found that the survival of *uqcc3*-knockdown zebrafish embryos was significantly diminished (Figure 2F).

These results indicate that the loss of *Uqcc3* impairs embryonic angiogenesis and induces apoptosis in normal conditions. These findings have prompted us to further explore the role of *Uqcc3* under pathological conditions.

UQCC3 deletion inhibits tumor angiogenesis and delays tumor growth

To investigate the role of *UQCC3* in tumor growth, we knocked out *UQCC3* in HepG2 cells and inoculated them into zebrafish. As expected, *UQCC3* knockout resulted in slower tumor growth accompanied by

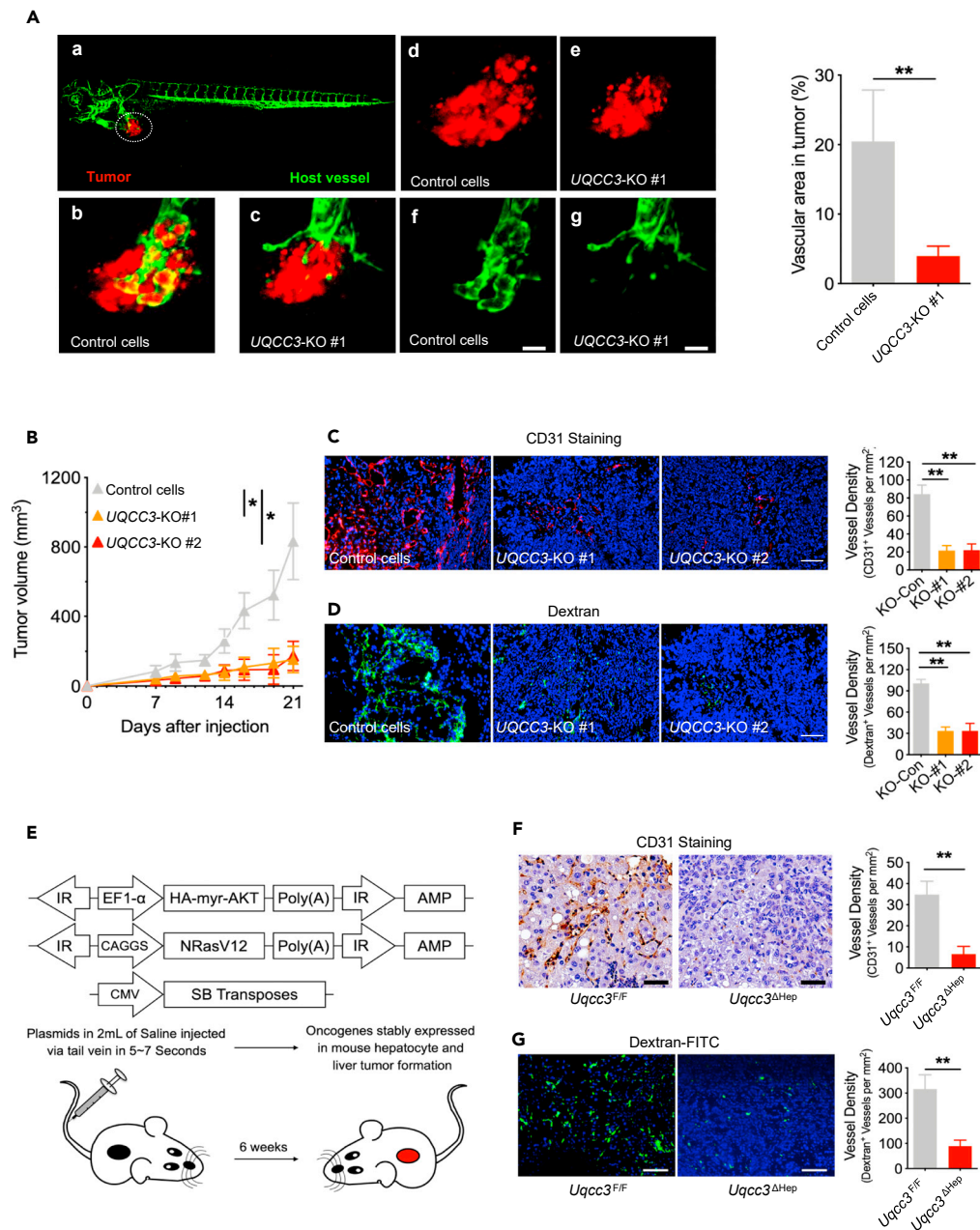


Figure 3. *Uqcc3* deletion impaired tumor angiogenesis and decreased tumor growth in zebrafish and mouse model

(A) Lateral view of a fluorescent transgenic Tg (flk1: EGFP) zebrafish embryo that was transplanted with cancer cells labeled with a red fluorescent dye. Scale bar: 200 μm . Data are represented as means \pm SEM. $**p < 0.01$, Student's *t* test.

(B) Reduction of HepG2 tumor growth in nude mice with *UQCC3*-KO compared with the control ($n = 5$). Data are represented as means \pm SEM. $*p < 0.05$, one-way ANOVA.

(C) Immunofluorescence staining of CD31 on subcutaneous tumors using specific antibodies directed against CD31 (left) and vessel density analysis (right). Scale bar: 200 μm . Data are represented as means \pm SEM. $**p < 0.01$, Student's *t* test.

(D) Subcutaneous tumor blood vessels were analyzed with FITC-dextran by confocal microscopy in control and *UQCC3*-KO tumors, and vessel density was analyzed. Scale bar: 200 μm . Data are represented as means \pm SEM. $**p < 0.01$, Student's *t* test.

(E) Experimental setup for the oncogene-primed HCC model by HDT with indicated plasmids into *Uqcc3*^{F/F} and *Uqcc3* ^{Δ Hep} mice with a C57BL/6 background.

Figure 3. Continued

(F) IHC staining of CD31 on HCC tissue using specific antibodies directed against CD31 (left) and vessel density analysis (right). Scale bar: 100 μm . Data are represented as means + SEM. $**p < 0.01$, Student's t test.

(G) Tumor blood vessels were analyzed with FITC-dextran by confocal microscopy in $Uqcc3^{F/F}$ and $Uqcc3^{\Delta\text{Hep}}$ mice (left) and vessel density analysis (right). Scale bar: 200 μm . Data are represented as means + SEM. $**p < 0.01$, Student's t test.

reduced angiogenesis in the tumor (Figure 3A). Next, we inoculated UQCC3-KO cell subcutaneously into immunodeficient mice; UQCC3 knockout resulted in slower tumor growth (Figure 3B). Meanwhile, vessel density was lower in UQCC3-knockout tumors, as shown by CD31 and Dextran-FITC staining (Figures 3C and 3D). To further determine the effect of UQCC3 on tumorigenesis and angiogenesis *in vivo*, we crossed mice from a floxed *Uqcc3* ($Uqcc3^{F/F}$) line with mice from an albumin-driven Cre recombinase deleter line (Alb-Cre), in which target genes can be specifically inactivated in hepatocytes ($Uqcc3^{\Delta\text{Hep}}$). We induced hepatocellular carcinoma (HCC) in $Uqcc3^{F/F}$ and $Uqcc3^{\Delta\text{Hep}}$ mice using hydrodynamic transfection (HDT) via the tail-vein injection of oncogenes myr-AKT and NRasV12²⁸ (Figure 3E). Six weeks after HDT, the HCC was established, and by CD31 staining, obvious blood vessels were visible in tumors from $Uqcc3^{F/F}$ mice but not from $Uqcc3^{\Delta\text{Hep}}$ mice (Figure 3F). To further confirm this phenomenon, we performed Dextran-FITC staining and obtained the same results (Figure 3G). These results suggest that UQCC3 is essential for tumor growth and tumor angiogenesis. Angiogenesis is mainly regulated by hypoxia and VEGF, and mitochondria are indispensable for this process. As UQCC3 is a mitochondrial protein, we speculate that UQCC3 regulates angiogenesis by regulating cellular adaptation to hypoxia.

UQCC3 stabilizes HIF-1 α under hypoxia and promotes angiogenesis

In many mammalian species, angiogenesis occurs in a hypoxic environment.²⁹ Is UQCC3 levels also associated with hypoxia? We first examined the hypoxia using a hypoxia probe and measured UQCC3 levels in tumor tissues. We found that UQCC3 is higher in the hypoxic region of the tumor (Figure 4A). To more directly confirm the effect of hypoxia on UQCC3 and HIF-1 α levels, we cultured tumor cells under 1% hypoxic conditions. The levels of HIF-1 α were significantly increased after hypoxia treatment, and the levels of UQCC3 were slightly increased after 4 h, but were further significantly increased after 8 h of hypoxia treatment (Figure 4B). In our *Uqcc3*-knockout mouse model, *Uqcc3* deletion led to a significant decrease in HIF-1 α intensity during embryo development (Figure 4C). In tumor cells, HIF-1 α levels was decreased after knockdown of UQCC3 under hypoxia (Figure 4D). Angiogenesis is driven by a set of angiogenic proteins, including angiogenic growth factors, chemokines, and extracellular matrix proteins. Among them, VEGF plays a dominant role,²¹ and HIF-1 α is a key regulator of VEGF. We detected the levels of VEGF in E9.5 embryos. As expected, in *Uqcc3*-deleted embryos, only a small proportion of cells expressed VEGF, and the expression levels were generally lower than in wild-type embryos (Figure 4E). In tumor cells, we also observed less VEGF secretion (Figure 4F). The tube formation assay represents an *in vitro* test to study the molecular mechanisms underlying the several steps that lead to the formation of new blood vessels. We performed tube formation experiments with human umbilical vein endothelial cells (HUVEC) in different conditions, including fresh medium, tumor cell culture medium with or without VEGF block, and UQCC3-knockout tumor cell culture medium with or without VEGF supplementation. HUVEC tube formation was impaired in UQCC3-knockout tumor cell culture medium, which can be rescued by VEGF supplementation (Figures 4G and 4H). Together, the data demonstrate that UQCC3 knockout leads to unstable HIF-1 α , decreased VEGF under hypoxia, and impaired angiogenesis.

UQCC3 regulates angiogenesis through the ROS/HIF/VEGF pathway

Since UQCC3 is a mitochondrial ETC complex assembly protein, we analyzed the effect of UQCC3 on mitochondrial function under hypoxia. Knockout of UQCC3 decreased cellular ATP content, mitochondrial mass, and membrane potential (Figures 5A–5C). As mitochondria are a major source of ROS, and mitochondrial ROS has important physiological roles,²⁵ we detected mitochondrial ROS using Mito SOX and found that mROS production was reduced in the absence of UQCC3 (Figure 5D). mROS is required and sufficient for HIF-1 α stabilization,⁷ and HIF-1 α regulates the expression of a suite of pro-angiogenic genes, such as VEGF.³⁰ We detected VEGF levels under normal or hypoxia conditions with UQCC3 knockout or overexpression. UQCC3 knockout or overexpression had no influence on VEGF under normal conditions. However, under hypoxia, UQCC3-KO resulted in decreased VEGF levels, and UQCC3 OE elevated VEGF levels (Figures 5E and 5F). We have known that the level of HIF-1 α is decreased after UQCC3 knockout under hypoxic conditions (Figures 4C and 4D), so we analyzed whether UQCC3 increases the levels of VEGF through HIF-1 α . As expected, VEGF levels increased by UQCC3 overexpression was abolished after HIF-1 α

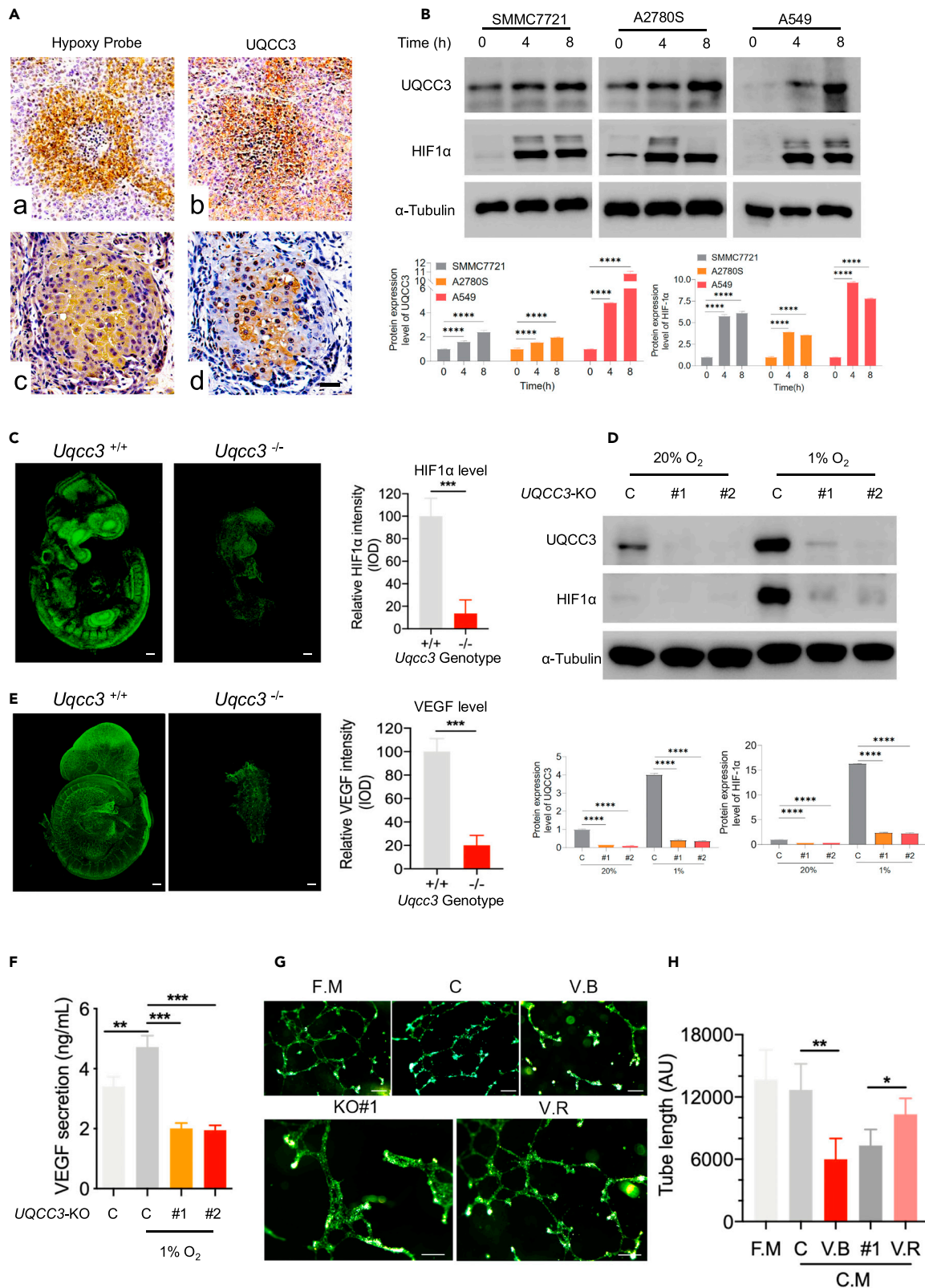


Figure 4. UQCC3 was highly expressed under hypoxia and important for HIF-1 α stabilization and VEGF expression

(A) Correlation analysis between representative hypoxia and UQCC3 levels in tumor tissues. Scale bar: 50 μ m.
 (B) Effect of hypoxia on UQCC3 levels and HIF-1 α activation. Three cell lines (SMMC7721, A2780S, and A549) were cultured under hypoxia for 0, 4, or 8 h. The lysates from the harvested cells were analyzed by immunoblotting. Data are represented as means +SEM. ****p < 0.0001, Student's t test.
 (C) HIF-1 α expression levels were detected in *Uqcc3*^{+/+} and *Uqcc3*^{-/-} mice using specific antibodies against HIF-1 α , and HIF-1 α intensity was analyzed (n = 5). Scale bar: 500 μ m. Data are represented as means +SEM. ***p < 0.001, Student's t test.
 (D) Western blot (WB) analysis was performed with the indicated antibodies on total cell extracts from WT or UQCC3-KO cells under normoxia (20% O₂) or hypoxia (1% O₂). Data are represented as means +SEM. ****p < 0.0001, Student's t test.
 (E) Immunofluorescent staining of VEGF in *Uqcc3*^{+/+} and *Uqcc3*^{-/-} embryos at E9.5. (Scale bars: 1 mm). VEGF-positive cells and relative VEGF intensity were analyzed (n = 3 for each group). Scale bar = 500 μ m. Data are represented as means +SEM. ***p < 0.001, Student's t test.
 (F) The secretion of VEGF in the supernatant by WT and UQCC3-KO cells was detected by ELISA. Data are represented as means +SEM. **p < 0.01, ***p < 0.001, Student's t test.
 (G) HUVECs were cultured on matrigel-coated 48-well plates for 18 h. Tube formation networks were observed under a microscope (Fresh medium: fresh medium for HUVEC growth, Condition media: tumor cell culture medium, VEGF block: tumor cell culture medium with VEGF block, UQCC3-KO: UQCC3-knockout tumor cell culture medium, UQCC3-KO+VEGF: UQCC3-knockout tumor cell culture medium with VEGF). Scale bar: 100 μ m.
 (H) Analysis of the total tube formation. Each bar represents the mean \pm SEM of three experiments compared to the control group. Data are represented as means +SEM. *p < 0.05, **p < 0.01, Student's t test.

knockdown (Figure 5G). We further investigated the effect of mROS on VEGF levels and found that UQCC3 overexpression could not increase VEGF levels after clearing mROS by Mito Q (Figure 5H). Based on the above results, we speculate that UQCC3 stabilizes HIF-1 α by increasing the production of mROS, thereby increasing the expression of VEGF and ultimately affecting angiogenesis. The results also showed that the expression of VEGF decreased after clearing mROS or knockdown of HIF-1 α , while overexpression of UQCC3 could not restore the expression of VEGF under this condition (Figure 5I). On the contrary, exogenous supplementation of ROS or overexpression of HIF-1 α could increase the expression of VEGF, and this increase was not affected by UQCC3 knockdown (Figure 5J). The above results indicate that UQCC3 can promote angiogenesis through the mROS-HIF-VEGF pathway.

UQCC3 expression is correlated with the progression and prognosis of tumor patients

To explore the role of UQCC3 in human tumor progression, we utilized the TCGA database to investigate the relationship between UQCC3 expression and tumor progression. To determine the expression levels of the UQCC3 gene in tumor and normal tissues, we used the TIMER2 web tool to analyze various cancer types in TCGA. We found that UQCC3 expression in 17 human tumor tissues, including LIHC (Liver hepatocellular carcinoma), LUAD (Lung adenocarcinoma), and LUSC (Lung squamous cell carcinoma), was significantly higher than in the corresponding normal control tissues (Figure 6A). The differential expression of UQCC3 between tumor and normal tissues suggests that UQCC3 plays an important role in regulating tumor development. Next, we used the GEPIA2 to study the correlation between UQCC3 expression levels and the pathological stages of cancers, including LIHC, THCA (Thyroid cancer), and BRCA, via the "pathological stage plot" module (Figure 6B). We also observed that upregulated UQCC3 expression was linked to poor prognosis and OS in many cancers, including ACC (adrenocortical carcinoma), KICH (kidney chromophobe), LIHC, MESO (mesothelioma), and LGG (brain lower grade glioma) (Figure 6C). These results indicate that the expression of UQCC3 plays an important role in the tumor development and prognosis of clinical patients.

DISCUSSION

Embryonic development and angiogenesis are controlled by complex regulatory networks, while mitochondria are indispensable regulators that are crucial for both embryogenesis and angiogenesis.³¹ In this study, we identified mitochondrial UQCC3 as a novel molecule controlling angiogenesis during embryonic development. We showed that ablation of *Uqcc3* in embryonic cells caused embryonic lethality in both mice and zebrafish. Furthermore, *Uqcc3* knockout significantly impaired embryonic angiogenesis, leading to a dramatic decrease in vessel branch points and density. These results demonstrated the important role of mitochondrial protein-mediated angiogenesis in embryonic development.

We assume that the regulation of angiogenesis by UQCC3 is ubiquitous under both physiological and pathological conditions. The process of tumor angiogenesis has been extensively studied,³² however, the upstream molecules regulating angiogenesis remain poorly understood. To elucidate the role of UQCC3 in tumor angiogenesis, we generated UQCC3-knockout tumor cell lines and developed a novel conditional knockout mouse model of *Uqcc3* deficiency that targeted liver cells via albumin-driven

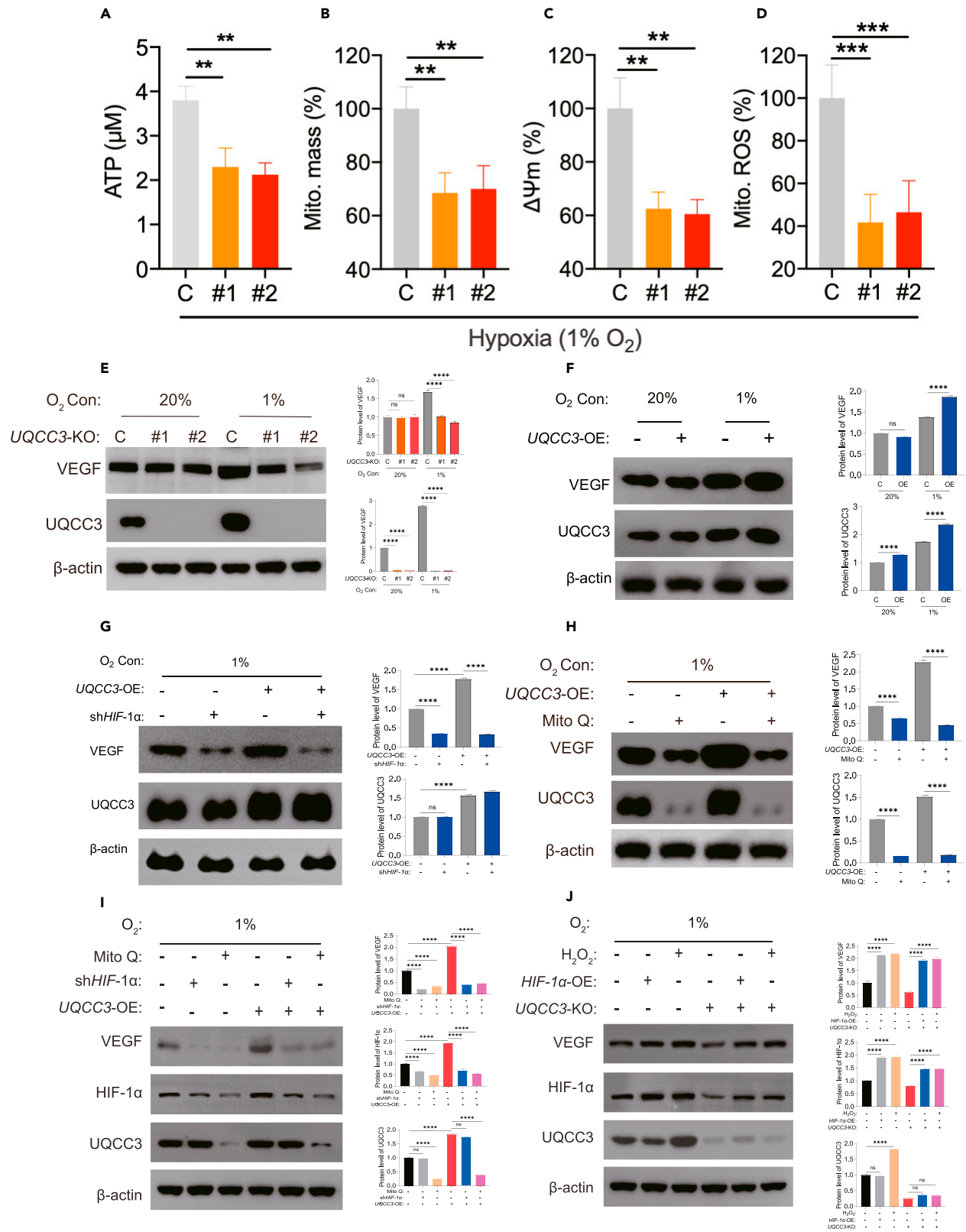


Figure 5. UQCC3 promoted VEGF expression through stabilize HIF-1 α under hypoxia by mROS

- (A) Representative ATP content in WT and UQCC3-KO cells under hypoxia (n = 6). Data are represented as means +SEM. **p < 0.01, Student's t test.
- (B) Representative relative proportion of mitochondrial mass in WT and UQCC3-KO cells. Mitochondrial mass is detected by the MitoTracker Green probe. Data are represented as means +SEM. **p < 0.01, Student's t test.
- (C) Representative relative proportion of mitochondrial membrane potential in WT and UQCC3-KO cells. Mitochondrial membrane potential is detected by TMRM. Data are represented as means +SEM. **p < 0.01, Student's t test.
- (D) Representative relative proportion of mROS in WT and UQCC3-KO cells. mROS is detected by the mitochondrial probe MitoSOX Red. Data are represented as means +SEM. ***p < 0.001, Student's t test.
- (E) Western blot analysis for UQCC3 and VEGF expression of UQCC3-KO and WT cells in normoxia and hypoxia conditions. Data are represented as means +SEM. ****p < 0.0001, Student's t test.
- (F) Representative UQCC3-OE influence on VEGF expression in normoxia and hypoxia conditions. Data are represented as means +SEM. ****p < 0.0001, Student's t test.
- (G) WB analysis of the expression of the VEGF protein in UQCC3-OE and WT cells with or without HIF-1 α knockdown in hypoxia condition. Data are represented as means +SEM. ****p < 0.0001, Student's t test.
- (H) WB analysis of the expression of the VEGF protein in UQCC3-OE and WT cells with or without ROS elimination by Mito Q in hypoxia condition. Data are represented as means +SEM. ****p < 0.0001, Student's t test.
- (I) Representative ROS elimination by Mito Q influence on VEGF expression in hypoxia of the indicated condition. Data are represented as means +SEM. ****p < 0.0001, Student's t test.
- (J) Representative ROS increased by H₂O₂ influence on VEGF expression in hypoxia of the indicated condition. Data are represented as means +SEM. ****p < 0.0001, Student's t test.

Cre-mediated deletion. UQCC3-knockout tumor cells inoculated into zebrafish or mice produced lower levels of tumor growth and angiogenesis than the parental cell line. Similarly, tumor angiogenesis in primary hepatic carcinomas induced in mice with liver-specific knockout of *Uqcc3* was significantly reduced compared with angiogenesis in tumors induced in wild-type mice. Our results suggest that UQCC3 may promote tumor angiogenesis by enhancing the secretion of pro-angiogenic factors by tumor cells.

We specifically hypothesized that UQCC3 may be required to enable tumor cells to adapt to hypoxic environments. Consistent with this notion, we found that UQCC3 expression was significantly increased in cells cultured under hypoxic conditions. Moreover, knockout of UQCC3 impaired mitochondrial function and suppressed the release of mitochondrial ROS, which are essential for HIF-1 α stabilization.¹⁹ Our results demonstrated that UQCC3 expression correlated strongly with hypoxia and HIF-1 α stabilization. UQCC3 deletion attenuated mitochondrial ROS production and HIF-1 α levels, while HIF-1 α levels were restored by exogenous supplementation of ROS. Moreover, in tube formation assays, the tubes induced by culture medium from UQCC3-knockout tumor cells were fewer in number and shorter in length than those induced by control medium. Activation of gene transcription by HIF-1 α involves dimerization with HIF-1 β in the nucleus followed by binding to hypoxia response elements in target genes,³³ most of which are involved in angiogenesis. One of the best-studied HIF-1 α -regulated angiogenic genes is VEGF.^{34,35} Our results showed that VEGF levels were decreased by UQCC3 deletion and rescued via ROS supplementation or HIF-1 α overexpression, indicating that UQCC3 acts as an upstream regulator of the ROS/HIF/VEGF signaling pathway.

As the largest resource in the field of cancer biology, TCGA aims to facilitate the identification of the molecular features of various cancer types.³⁶ To explore the relationship between UQCC3 expression and clinical status, we used TCGA data to examine UQCC3 expression in tumor and normal tissues. We found that UQCC3 expression was closely related to various tumors, including LIHC, BRCA, and THCA. Moreover, using the GEPIA database, we found that UQCC3 expression was positively correlated with pathological stage in these tumor types and that higher expression of UQCC3 led to shorter overall survival times. These results indicate that UQCC3 can be used as a new molecular marker for predicting tumor development.

Angiogenesis plays a critical role in anti-tumor therapy. Accordingly, inhibition of tumor angiogenesis via blockade of the HIF-1 α /VEGF/VEGFR-signaling pathway has been explored as a potential therapeutic approach for solid tumors. Indeed, several anti-angiogenic agents approved for cancer treatment rely on targeting VEGF or VEGFRs and have achieved great success.²⁹ Interestingly, recent computational and experimental models have shown that normalizing tumor blood vessels leads to a reduction in microvascular density, which itself reduces interstitial fluid pressure in tumor tissues. This phenomenon ultimately induces the prerequisite physiological conditions for the subsequent distribution and intracellular penetration of therapeutic agents within the tumor tissue.^{37,38} These findings underscore the significance of angiogenesis and vascular normalization in anti-angiogenic therapy and the efficacy of drug delivery systems.

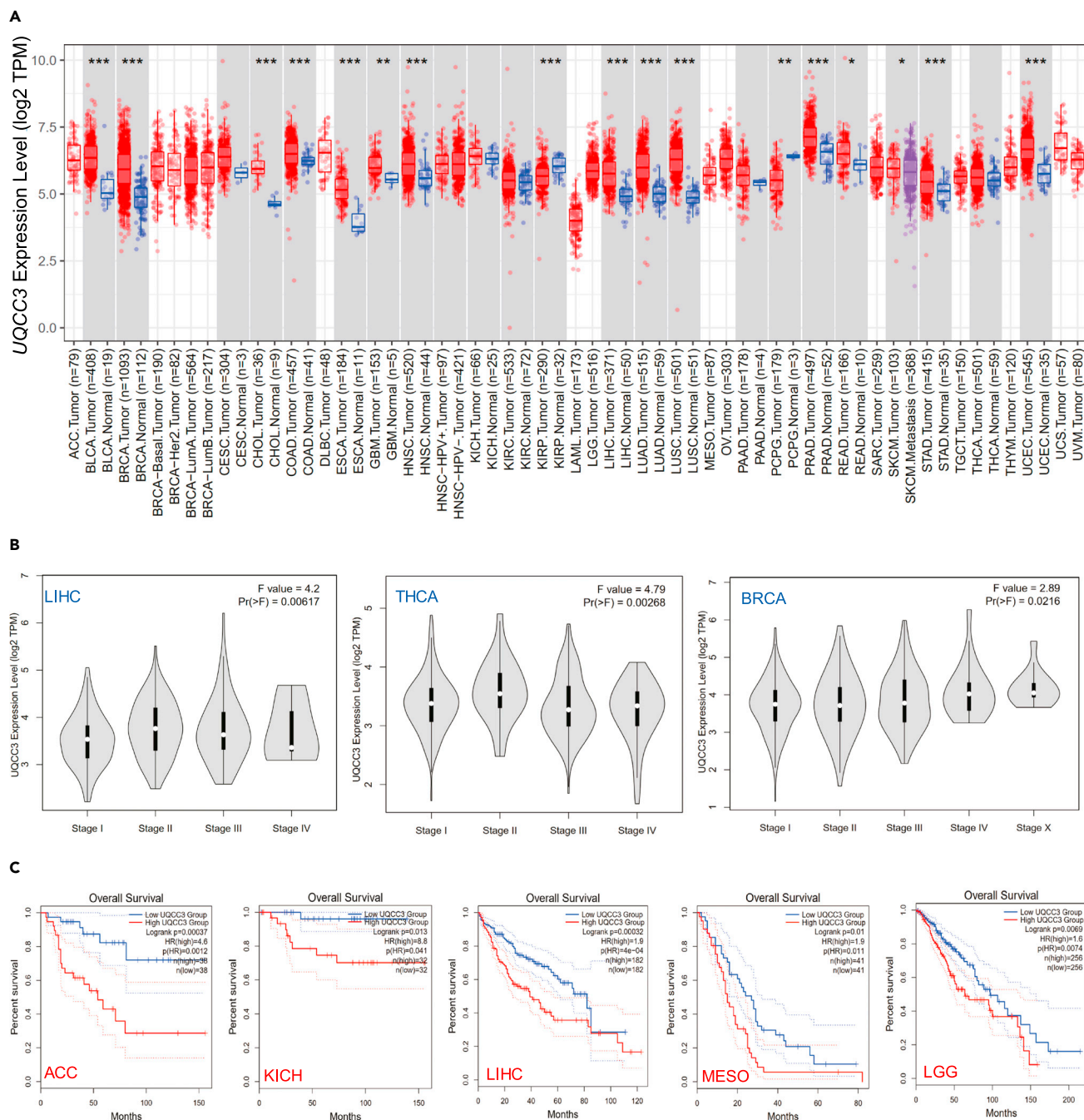


Figure 6. UQC3 expression is correlated with the progression and prognosis of tumor

(A) The TCGA project's UQC3 gene expression difference in different tumors or specific tumor subtype tissues and adjacent normal tissues was analyzed by TIMER2. * $p < 0.05$, ** $p < 0.01$, *** $p < 0.001$, Wilcoxon test.

(B) Using TCGA data, UQC3 gene expression was analyzed by main pathological stage (stage I, stage II, stage III, stage IV, and stage X) of LIHC, THCA, and BRCA. Log₂ (TPM + 1) was used for the log scale.

(C) The overall survival rate, as well as UQC3 gene expression in different tumors in TCGA, was analyzed by GEPIA2 software. The survival diagram and Kaplan-Meier curves with positive results are shown.

Our results reveal a novel role for UQC3 in the regulation of angiogenesis within the tumor microenvironment and suggest that molecules targeting anti-UQC3 could be developed as potential drug leads for cancer therapy.

In summary, the generation of *Uqc3*-deficient mice has allowed us to identify the essential roles of this mitochondrial complex III assembly protein in embryonic and tumor development. We identified UQCC3 as a key factor affecting mitochondrial ROS production, which in turn regulates HIF-1 α stability and VEGF secretion under hypoxic conditions, ultimately affecting angiogenesis. These findings provide new perspectives for the development of cancer therapies and emphasize the importance of studying genetics and mitochondria in tumor cells when considering mechanisms of cancer development and potential therapeutic approaches.

Limitations of the study

Although our study demonstrated embryonic lethality and impaired angiogenesis in *Uqc3*-knockout mice and zebrafish, the effect of UQCC3 on human embryonic development remains unknown. In addition, further research is required to clarify the detailed molecular mechanisms underlying the effects of UQCC3 on mitochondrial ROS generation. The identification of UQCC3 as a potential therapeutic target for anti-angiogenesis also requires validation.

STAR★METHODS

Detailed methods are provided in the online version of this paper and include the following:

- KEY RESOURCES TABLE
- RESOURCE AVAILABILITY
 - Lead contact
 - Materials availability
 - Data and code availability
- EXPERIMENTAL MODELS AND STUDY PARTICIPANT DETAILS
 - Mice
 - Zebrafish
 - Cell culture
- METHOD DETAILS
 - Xenograft models
 - Human umbilical vein endothelial cell isolation and culture
 - Tube formation assay
 - Western blot
 - ATP determination
 - Mitochondrial function assays
 - Immunohistochemistry
 - Whole mount fluorescent immunohistochemistry
- QUANTIFICATION AND STATISTICAL ANALYSIS

SUPPLEMENTAL INFORMATION

Supplemental information can be found online at <https://doi.org/10.1016/j.isci.2023.107370>.

ACKNOWLEDGMENTS

This project was supported by grants from Natural Science Funding of China (81171956, 81772605, and 81572402), the 70th batch of general funding list of China Postdoctoral Science Foundation(2021M702327), the Sichuan University postdoctoral interdisciplinary Innovation Fund and the 1.3.5 project for disciplines of excellence, West China Hospital, Sichuan University (ZYJC18008).

AUTHOR CONTRIBUTIONS

G.M.-Z. performed most experiments with the assistance of Y.-Y., B.R.-L., S.-X., L.C.-C., H.-L., J.-Z., Y.H.-W., F.Z.-G., J.-G., F.-Z., L.-X., Q.Q.-L., Y.G.-S., H.J.-Z., Y.-L., and R.-L. H.S.-Y., and Y.-Y. conceived the project, designed the experiments, G.M.-Z., Y.-Y., and B.R.-L. analyzed and interpreted the data. G.M.-Z., Y.-Y., B.R.-L., H.X.-D. and H.S.-Y. wrote the manuscript. All authors had the opportunity to discuss the results and comment on the manuscript.

DECLARATION OF INTERESTS

None.

INCLUSION AND DIVERSITY

We support inclusive, diverse, and equitable conduct of research.

Received: March 16, 2023

Revised: June 5, 2023

Accepted: July 10, 2023

Published: July 13, 2023

REFERENCES

- Jaykumar, A.B., Plumber, S., Barry, D.M., Binns, D., Wichaidit, C., Grzemska, M., Earnest, S., Goldsmith, E.J., Cleaver, O., and Cobb, M.H. (2022). WNK1 collaborates with TGF-beta in endothelial cell junction turnover and angiogenesis. *Proc. Natl. Acad. Sci. USA* 119, e2203743119. <https://doi.org/10.1073/pnas.2203743119>.
- Li, H., Liu, P., Li, D., Wang, Z., Ding, Z., Zhou, M., Chen, X., Miao, M., Ding, J., Lin, W., et al. (2022). STAT3/miR-130b-3p/MBNL1 feedback loop regulated by mTORC1 signaling promotes angiogenesis and tumor growth. *J. Exp. Clin. Cancer Res.* 41, 297. <https://doi.org/10.1186/s13046-022-02513-z>.
- Wang, C., Dai, X., Wu, S., Xu, W., Song, P., and Huang, K. (2021). FUNDC1-dependent mitochondria-associated endoplasmic reticulum membranes are involved in angiogenesis and neoangiogenesis. *Nat. Commun.* 12, 2616. <https://doi.org/10.1038/s41467-021-22771-3>.
- Lee, H.W., Xu, Y., He, L., Choi, W., Gonzalez, D., Jin, S.W., and Simons, M. (2021). Role of Venous Endothelial Cells in Developmental and Pathologic Angiogenesis. *Circulation* 144, 1308–1322. <https://doi.org/10.1161/CIRCULATIONAHA.121.054071>.
- Lv, X., Li, J., Zhang, C., Hu, T., Li, S., He, S., Yan, H., Tan, Y., Lei, M., Wen, M., and Zuo, J. (2017). The role of hypoxia-inducible factors in tumor angiogenesis and cell metabolism. *Genes Dis.* 4, 19–24. <https://doi.org/10.1016/j.gendis.2016.11.003>.
- Kierans, S.J., and Taylor, C.T. (2021). Regulation of glycolysis by the hypoxia-inducible factor (HIF): implications for cellular physiology. *J. Physiol.* 599, 23–37. <https://doi.org/10.1113/JP280572>.
- Manuelli, V., Pecorari, C., Filomeni, G., and Zito, E. (2022). Regulation of redox signaling in HIF-1-dependent tumor angiogenesis. *FEBS J.* 289, 5413–5425. <https://doi.org/10.1111/febs.16110>.
- Simons, M., Gordon, E., and Claesson-Welsh, L. (2016). Mechanisms and regulation of endothelial VEGF receptor signalling. *Nat. Rev. Mol. Cell Biol.* 17, 611–625. <https://doi.org/10.1038/nrm.2016.87>.
- Kashkooli, F.M., Abazari, M.A., Soltani, M., Ghazani, M.A., and Rahmim, A. (2022). A spatiotemporal multi-scale computational model for FDG PET imaging at different stages of tumor growth and angiogenesis. *Sci. Rep.* 12, 10062. <https://doi.org/10.1038/s41598-022-13345-4>.
- Huang, X., Zhao, L., and Peng, R. (2022). Hypoxia-Inducible Factor 1 and Mitochondria: An Intimate Connection. *Biomolecules* 13, 50. <https://doi.org/10.3390/biom13010050>.
- Bao, X., Zhang, J., Huang, G., Yan, J., Xu, C., Dou, Z., Sun, C., and Zhang, H. (2021). The crosstalk between HIFs and mitochondrial dysfunctions in cancer development. *Cell Death Dis.* 12, 215. <https://doi.org/10.1038/s41419-021-03505-1>.
- Hamanaka, R.B., and Chandel, N.S. (2009). Mitochondrial reactive oxygen species regulate hypoxic signaling. *Curr. Opin. Cell Biol.* 21, 894–899. <https://doi.org/10.1016/j.ceb.2009.08.005>.
- Chandel, N.S., McClintock, D.S., Feliciano, C.E., Wood, T.M., Melendez, J.A., Rodriguez, A.M., and Schumacker, P.T. (2000). Reactive oxygen species generated at mitochondrial complex III stabilize hypoxia-inducible factor-1alpha during hypoxia: a mechanism of O2 sensing. *J. Biol. Chem.* 275, 25130–25138. <https://doi.org/10.1074/jbc.M001914200>.
- Kurelac, I., Iommarini, L., Vatrinet, R., Amato, L.B., De Luise, M., Leone, G., Girolimetti, G., Umesh Ganesh, N., Bridgeman, V.L., Ombrato, L., et al. (2019). Inducing cancer indolence by targeting mitochondrial Complex I is potentiated by blocking macrophage-mediated adaptive responses. *Nat. Commun.* 10, 903. <https://doi.org/10.1038/s41467-019-08839-1>.
- Bastian, A., Matsuzaki, S., Humphries, K.M., Pharaoh, G.A., Doshi, A., Zaware, N., Gangjee, A., and Ilnat, M.A. (2017). AG311, a small molecule inhibitor of complex I and hypoxia-induced HIF-1alpha stabilization. *Cancer Lett.* 388, 149–157. <https://doi.org/10.1016/j.canlet.2016.11.040>.
- Nakhle, J., Rodriguez, A.M., and Vignais, M.L. (2020). Multifaceted Roles of Mitochondrial Components and Metabolites in Metabolic Diseases and Cancer. *Int. J. Mol. Sci.* 21, 4405. <https://doi.org/10.3390/ijms21124405>.
- Yang, J., Ren, B., Yang, G., Wang, H., Chen, G., You, L., Zhang, T., and Zhao, Y. (2020). The enhancement of glycolysis regulates pancreatic cancer metastasis. *Cell. Mol. Life Sci.* 77, 305–321. <https://doi.org/10.1007/s00018-019-03278-z>.
- Bleier, L., and Dröse, S. (2013). Superoxide generation by complex III: from mechanistic rationales to functional consequences. *Biochim. Biophys. Acta* 1827, 1320–1331. <https://doi.org/10.1016/j.bbabi.2012.12.002>.
- Willson, J.A., Arienti, S., Sadiku, P., Reyes, L., Coelho, P., Morrison, T., Rinaldi, G., Dockrell, D.H., Whyte, M.K.B., and Walmsley, S.R. (2022). Neutrophil HIF-1alpha stabilization is augmented by mitochondrial ROS produced via the glycerol 3-phosphate shuttle. *Blood* 139, 281–286. <https://doi.org/10.1182/blood.20211011010>.
- Klimova, T., and Chandel, N.S. (2008). Mitochondrial complex III regulates hypoxic activation of HIF. *Cell Death Differ.* 15, 660–666. <https://doi.org/10.1038/sj.cdd.4402307>.
- Reichard, A., and Asosingh, K. (2019). The role of mitochondria in angiogenesis. *Mol. Biol. Rep.* 46, 1393–1400. <https://doi.org/10.1007/s11033-018-4488-x>.
- Desmurs, M., Foti, M., Raemy, E., Vaz, F.M., Martinou, J.C., Bairoch, A., and Lane, L. (2015). C11orf83, a mitochondrial cardiolipin-binding protein involved in bc1 complex assembly and supercomplex stabilization. *Mol. Cell Biol.* 35, 1139–1156. <https://doi.org/10.1128/mcb.01047-14>.
- Wanschers, B.F.J., Szklarczyk, R., van den Brand, M.A.M., Jonckheere, A., Suijskens, J., Smeets, R., Rodenburg, R.J., Stephan, K., Helland, I.B., Elkamil, A., et al. (2014). A mutation in the human CBP4 ortholog UQCC3 impairs complex III assembly, activity and cytochrome b stability. *Hum. Mol. Genet.* 23, 6356–6365. <https://doi.org/10.1093/hmg/ddu357>.
- Liang, C., Zhang, S., Robinson, D., Ploeg, M.V., Wilson, R., Nah, J., Taylor, D., Beh, S., Lim, R., Sun, L., et al. (2022). Mitochondrial microproteins link metabolic cues to respiratory chain biogenesis. *Cell Rep.* 40, 111204. <https://doi.org/10.1016/j.celrep.2022.111204>.
- Yang, Y., Zhang, G., Guo, F., Li, Q., Luo, H., Shu, Y., Shen, Y., Gan, J., Xu, L., and Yang, H. (2020). Mitochondrial UQCC3 Modulates Hypoxia Adaptation by Orchestrating OXPHOS and Glycolysis in Hepatocellular Carcinoma. *Cell Rep.* 33, 108340. <https://doi.org/10.1016/j.celrep.2020.108340>.
- Zhang, P.C., Liu, X., Li, M.M., Ma, Y.Y., Sun, H.T., Tian, X.Y., Wang, Y., Liu, M., Fu, L.S., Wang, Y.F., et al. (2020). AT-533, a novel Hsp90 inhibitor, inhibits breast cancer growth and HIF-1alpha/VEGF/VEGFR-2-mediated angiogenesis in vitro and in vivo. *Biochem. Pharmacol.* 172, 113771. <https://doi.org/10.1016/j.bcp.2019.113771>.
- Movafagh, S., Crook, S., and Vo, K. (2015). Regulation of hypoxia-inducible factor-1a by

- reactive oxygen species: new developments in an old debate. *J. Cell. Biochem.* 116, 696–703. <https://doi.org/10.1002/jcb.25074>.
28. Chen, X., and Calvisi, D.F. (2014). Hydrodynamic transfection for generation of novel mouse models for liver cancer research. *Am. J. Pathol.* 184, 912–923. <https://doi.org/10.1016/j.ajpath.2013.12.002>.
 29. Lopes-Coelho, F., Martins, F., Pereira, S.A., and Serpa, J. (2021). Anti-Angiogenic Therapy: Current Challenges and Future Perspectives. *Int. J. Mol. Sci.* 22, 3765. <https://doi.org/10.3390/ijms22073765>.
 30. Korbecki, J., Kojder, K., Kapczuk, P., Kupnicka, P., Gawrońska-Szklarz, B., Gutowska, I., Chlubek, D., and Baranowska-Bosiacka, I. (2021). The Effect of Hypoxia on the Expression of CXC Chemokines and CXC Chemokine Receptors-A Review of Literature. *Int. J. Mol. Sci.* 22, 843. <https://doi.org/10.3390/ijms22020843>.
 31. Herkenne, S., Ek, O., Zamberlan, M., Pellattiero, A., Chergova, M., Chivite, I., Novotná, E., Rigoni, G., Fonseca, T.B., Samardzic, D., et al. (2020). Developmental and Tumor Angiogenesis Requires the Mitochondria-Shaping Protein Opa1. *Cell Metabol.* 31, 987–1003.e8. <https://doi.org/10.1016/j.cmet.2020.04.007>.
 32. Al-Ostoot, F.H., Salah, S., Khamees, H.A., and Khanum, S.A. (2021). Tumor angiogenesis: Current challenges and therapeutic opportunities. *Cancer Treat. Res. Commun.* 28, 100422. <https://doi.org/10.1016/j.ctarc.2021.100422>.
 33. Rankin, E.B., and Giaccia, A.J. (2016). Hypoxic control of metastasis. *Science (New York, N.Y.)* 352, 175–180. <https://doi.org/10.1126/science.aaf4405>.
 34. Jabari, M., Allahbakhshian Farsani, M., Salari, S., Hamidpour, M., Amiri, V., and Mohammadi, M.H. (2019). Hypoxia-Inducible Factor1-A (HIF1 α) and Vascular Endothelial Growth Factor-A (VEGF-A) Expression in De Novo AML Patients. *Asian Pac. J. Cancer Prev. APJCP* 20, 705–710. <https://doi.org/10.31557/apjcp.2019.20.3.705>.
 35. Hu, K., Babapoor-Farrokhran, S., Rodrigues, M., Deshpande, M., Puchner, B., Kashiwabuchi, F., Hassan, S.J., Asnaghi, L., Handa, J.T., Merbs, S., et al. (2021). Correction: Hypoxia-inducible factor 1 upregulation of both VEGF and ANGPTL4 is required to promote the angiogenic phenotype in uveal melanoma. *Oncotarget* 12, 519–520. <https://doi.org/10.18632/oncotarget.27780>.
 36. Krasnov, G.S., Kudryavtseva, A.V., Snezhkina, A.V., Lakunina, V.A., Beniaminov, A.D., Melnikova, N.V., and Dmitriev, A.A. (2019). Pan-Cancer Analysis of TCGA Data Revealed Promising Reference Genes for qPCR Normalization. *Front. Genet.* 10, 97. <https://doi.org/10.3389/fgene.2019.00097>.
 37. Abazari, M.A., Soltani, M., and Kashkooli, F.M. (2023). Targeted nano-sized drug delivery to heterogeneous solid tumor microvasculatures: Implications for immunoliposomes exhibiting bystander killing effect. *Phys. Fluids* 35, 011905. <https://doi.org/10.1063/5.0130259>.
 38. Mpekris, F., Voutouri, C., Panagi, M., Baish, J.W., Jain, R.K., and Stylianopoulos, T. (2022). Normalizing tumor microenvironment with nanomedicine and metronomic therapy to improve immunotherapy. *J. Contr. Release* 345, 190–199. <https://doi.org/10.1016/j.jconrel.2022.03.008>.
 39. Kotch, L.E., Iyer, N.V., Laughner, E., and Semenza, G.L. (1999). Defective vascularization of HIF-1 α -null embryos is not associated with VEGF deficiency but with mesenchymal cell death. *Dev. Biol.* 209, 254–267. <https://doi.org/10.1006/dbio.1999.9253>.

STAR★METHODS

KEY RESOURCES TABLE

REAGENT or RESOURCE	SOURCE	IDENTIFIER
Antibodies		
HIF-1 α	BD Biosciences	Cat# 610959; RRID: AB_398272
VEGF	Abcam	Cat# ab52917; RRID:AB_883427
β -Actin	Beyotime	Cat# AF0003; RRID:AB_2893353
α -Tubulin	Beyotime	Cat# AF0001; RRID:AB_2938690
CD31	Abcam	Cat# ab42232; RRID:AB_2161032
Goat Anti-Rabbit IgG (H+L) Antibody, Alexa Fluor 488 Conjugated	Thermo Fisher	Cat# A-11008; RRID:AB_143165
Goat Anti-Rabbit IgG (H+L) Antibody, Alexa Fluor 594 Conjugated	Thermo Fisher	Cat# A-11012; RRID:AB_141359
Chemicals, peptides, and recombinant proteins		
Fetal Bovine Serum (FBS)	Invitrogen	Cat# 10099141
Penicillin-streptomycin	Invitrogen	Cat# 15070063
Trypsin	Invitrogen	Cat# 15090046
Matrigel	Corning	Cat# 354234
RIPA Buffer	Cell Signaling Technology	Cat# 9806
PVDF	Invitrogen	Cat# 88518
Clarity Western ECL Substrate	Bio-Rad	Cat #1705061
MitoSOX™	Invitrogen	Cat# M36005
Formaldehyde solution	Sigma	Cat# 252549
Triton™ X-100	Sigma	Cat# 93443
Sodium azide	Sigma	Cat# 104760
TaqMan™ Fast Advanced Master Mix	Thermo Fisher	Cat# 4444557
DMEM medium	Invitrogen	Cat# 12800017, Lot No. 2248833
PBS	Invitrogen	Cat# 10010023
Protease inhibitor cocktail	Beyotime	Cat# P1005
Critical commercial assays		
ATP Determination Kit	Thermo Fisher	Cat# A22066
MitoTracker™ Green FM	Invitrogen	Cat# M46750
MitoProbe™ TMRM	Invitrogen	Cat# M20036
Experimental models: Cell lines		
A2780S	Sigma	Cat# CB_93112519; RRID:CVCL_0134
A549	ATCC	Cat# CRM-CCL-185; RRID:CVCL_0023
HepG2	ATCC	Cat# HB-8065; RRID:CVCL_0027
SMMC-7721	Beyotime	Cat# C6865; RRID:CVCL_0534
Oligonucleotides		
Primers for PCR, See Table S1	This paper	N/A
Software and algorithms		
Image J	NIH	https://imagej.nih.gov/ij/
Prism	Graphpad	https://www.graphpad.com/scientificsoftware/prism/
TIMER2	TCGA	http://timer.cistrome.org/
GEPIA2	TCGA	http://gepia2.cancer-pku.cn/#index

RESOURCE AVAILABILITY

Lead contact

Further information and requests for resources and reagents should be directed to and will be fulfilled by the lead contact Prof. Hanshuo Yang (yhansh@scu.edu.cn).

Materials availability

This study did not generate new unique reagents.

Data and code availability

- This paper analyses existing, publicly available data, all data presented in this study can be found in <http://timer.cistrome.org/> and <http://gepia2.cancer-pku.cn/#index>
- This paper does not report original code.
- Any additional information required to reanalyze the data reported in this paper is available from the [lead contact](#) upon request.

EXPERIMENTAL MODELS AND STUDY PARTICIPANT DETAILS

Mice

Wild-type C57BL/6 and nude mice were purchased from Beijing Vital River Laboratory Animal Technology Co., Ltd. *Uqcc3*^{+/-} mice and homozygous *Uqcc3* loxP (*Uqcc3*^{F/F}) mice were produced by Beijing View Solid Biotechnology Co., Ltd. *Uqcc3*^{F/F} mice were crossed with Alb-Cre mice (Jackson no. 003574) to generate *Uqcc3*^{ΔHep} mice. Male and female mice aged 6-8 weeks were used for tumor inoculation. To investigate embryonic development and embryonic angiogenesis, male and female mice aged 10-12 weeks were allowed to mate overnight. The following day, female mice were examined for the presence of copulation plugs and then separated from the males. Mice were maintained under pathogen-free conditions at the Sichuan University Laboratory Animal Center. All animal experiments were approved by the Committee for Animal Research at the Experimental and Research Animal Institute of Sichuan University. The primers used for genotyping PCR are in [Table S1](#).

Zebrafish

Tg(flk1:EGFP) zebrafish were maintained under normal conditions of 28°C, pH 7.2-7.4, and a 14-hour on/10-hour off light cycle. The embryos used for gene knockout experiments were within 0.5 hours post-fertilization at developmental age, while embryos 48 hours post-fertilization were used for tumor inoculation. The influence of sex is not reported in embryos at this point in development because embryos are not sexually differentiated.

Cell culture

A2780S (a human ovarian cancer cell line, ATCC), A549 (a human epithelial cell line derived from lung carcinoma, ATCC), and SMMC-7721 (a human hepatocellular carcinoma cell line, ATCC) cells were cultured in Dulbecco's Modified Eagle Medium (DMEM, Gibco), supplemented with 10% fetal bovine serum (FBS, Gibco), and 1% penicillin-streptomycin (Gibco). All cells were cultured at 37°C in a 5% CO₂ atmosphere. For hypoxia treatment, cells were cultured under hypoxic conditions (1% O₂) in a hypoxic incubator (Thermo Fisher Scientific).

METHOD DETAILS

Xenograft models

For xenograft models, 5×10⁶ HepG2 cells with or without *UQCC3* deletion were xenografted into the subcutaneous region of nude mice. After five days, tumor volumes were monitored three times a week to observe the dynamic development of tumor growth. The tumor volume was calculated using the following formula: 0.52×length×width². Three weeks post-inoculation, the mice were euthanized. The tumors were dissected out, weighed, fixed in 10% formalin, and frozen in liquid nitrogen for further analysis.

Human umbilical vein endothelial cell isolation and culture

Endothelial cells were isolated from human umbilical cord veins (HUVEC) as previously described.³⁹ A 0.2% collagenase (Sigma) solution was injected into the vein and clamped tightly with a surgical clamp before

incubation in a water bath for 10 minutes. The cord was then gently squeezed to facilitate cell detachment, and the cells were collected by washing the vein with phosphate-buffered saline. The cell pellet was suspended in M199 medium with 20% fetal calf serum (Gibco) and cultured in a 37°C, 5% CO₂ incubator (Thermo Fisher Scientific). The next day (less than 24 hours later), non-adherent cells were removed by changing the culture medium. A solution of 0.25% trypsin (Gibco) was used for cell subculture.

Tube formation assay

Tube formation was assessed using the Matrigel assay. Briefly, Matrigel (Corning Incorporated) was thawed on ice overnight and spread evenly over each well (300 µL) of a 24-well plate. The plate was then allowed to set for 30 minutes at 37°C. Subsequently, 4×10^4 HUVECs/well were seeded on top of the matrix and grown in 300 µL of complete growth media for 16 hours at 37°C and 5% CO₂. Images were taken using a confocal microscope (Zeiss LSM 880), and the tube length was identified and analyzed using the "Angiogenesis Analyzer" plugin for ImageJ.

Western blot

Western blot analysis was performed using standard procedures. In brief, whole-cell extracts were prepared using RIPA buffer. After electrophoresis, proteins were transferred onto a polyvinylidene difluoride (PVDF) membrane (Invitrogen) at 120 Volts. Indicated primary antibodies were used. Protein bands were visualized by an enhanced chemiluminescence assay kit (Bio-rad). The following antibodies were used: Human UQCC3 (customized by Abmart), HIF-1 α (BD Biosciences, #610959), VEGF (Abcam, ab52917), β -Actin (Beyotime, AF0003), and α -Tubulin (Beyotime, AF0001).

ATP determination

The ATP concentrations were analyzed using targeted metabolomics or the ATP Determination Kit (Molecular Probes). For the kit, a standard curve was drawn, and the ATP concentration of all samples was normalized to the total protein content evaluated by the Bradford assay.

Mitochondrial function assays

Mitochondrial mass, mitochondrial membrane potential, and mitochondrial ROS were detected using MitoTracker™ Green FM (Invitrogen), MitoProbe™ TMRM (Invitrogen), and MitoSOX™ (Invitrogen) according to the manufacturer's instructions. Briefly, 1×10^6 cells were stained with 100 nM MitoTracker Green, 20 nM TMRM, or 500 nM MitoSOX for 30 minutes at 37°C with 5% CO₂. After being washed with PBS, the cells were analyzed on a flow cytometer with appropriate excitation and emission wavelengths.

Immunohistochemistry

Xenograft and HDT-induced liver cancer tissues were fixed in 10% formaldehyde solution (Sigma), processed, embedded in paraffin, and sliced into 4-µm sections. The slides were subjected to H&E or IHC staining in the Laboratory of Pathology (West China Hospital, Sichuan University, China). To ensure antibody specificity, PBS was used as a negative control to replace the primary antibody. The density of IHC staining was determined using Image Pro Plus 6.0 software.

Whole mount fluorescent immunohistochemistry

Place the embryo in a 5 ml bijou with 4% paraformaldehyde and leave it to fix at 4°C overnight. Wash it three times in PBS with 0.5-1% Triton for 30 minutes each time. Incubate the embryos twice for 1 hour in blocking buffer (PBS with 1% Triton, 10% FCS, and 0.2% sodium azide) at room temperature. Transfer the embryos to a 2 ml tube and add the primary antibodies (mouse anti-CD31 (1:100; Abcam) and rabbit anti-UQCC3 (1:100; Abmart, customization)), and incubate for 2 days. After washing the embryos several times, add the secondary antibodies (Alexa Fluor 488 goat anti-Rabbit IgG and Alexa Fluor 594 goat anti-rabbit IgG (both 1:1000; Invitrogen)) in the blocking buffer (PBS with 1% Triton, 10% FCS, and 0.2% sodium azide), and incubate for 2 days. Then wash them several times, mount and view the embryos, and store them at 4°C in the dark until analysis. Ten representative non-overlapping confocal images were obtained with a LSM880 Meta Laser Scanning microscope at 630 \times magnification (Zeiss, Oberkochen, Germany). ImageJ software was used to quantify protein in a blinded manner, measuring the average and the area of fluorescence intensity at the apical pole.

QUANTIFICATION AND STATISTICAL ANALYSIS

Quantification and statistical analysis Statistical parameters including the exact value of n , (mean \pm SEM) and statistical significance are reported in the Figures and Figure Legends. Data graphics and statistical analyses were performed using Prism 9 (GraphPad). Statistical significance between two groups was analyzed using the unpaired Student's t test. Survival analysis used the Kaplan-Meier method. Three or more groups were analyzed by one-way ANOVA followed by Tukey's post hoc test. Statistical significance is denoted as follows: * $p < 0.05$, ** $p < 0.01$, *** $p < 0.001$, and **** $p < 0.0001$.